Journal of
Sensor and Actuator Networks

MDPI

Article

An Automated Semantic Segmentation Methodology for Infrared Thermography Analysis of the Human Hand

Melchior Arnal [1,2,3,*], Cyprien Bourrilhon [3,4], Vincent Beauchamps [3,5], Fabien Sauvet [3,5], Hassan Zahouani [6] and Coralie Thieulin [1,6]

1 LyRIDS, ECE Paris, 10 Rue Sextius Michel, 75015 Paris, France
2 RACER 1927, 1 rue de la Forge, 13300 Salon-de-Provence, France
3 Institut de Recherche Biomédicale des Armées, 1 Place Général Valérie André, 91223 Brétigny sur Orge, France; cbourrilhon@gmail.com (C.B.); vincent.beauchamps.pro@gmail.com (V.B.); fabien.sauvet@gmail.com (F.S.)
4 UMR LBEPS, Université Evry Paris-Saclay, 28 Bd François Mitterand, 91000 Evry-Courcouronnes, France
5 URP 7330 VIFASOM, Université Paris Cité, Hôtel Dieu, Parvis Notre Dame, 74004 Paris, France
6 Laboratoire de Tribologie et Dynamique des Systèmes, Ecole Centrale de Lyon, UMR-CNRS 5513, 69134 Lyon, France; hassan.zahouani@ec-lyon.fr (H.Z.); cthieulin@ece.fr (C.T.)
* Correspondence: melchior.arnal@edu.ece.fr

Abstract: Infrared thermography is a non-invasive measurement method that can accurately describe immediate temperature changes of an object. In the case of continuous in vivo hand measurements, extracting correct thermal data requires a first step of image segmentation to identify regions of interest. This step can be difficult due to parasitic hand movements. It is therefore necessary to regularly readjust the segmented areas throughout the recording. This process is time-consuming and presents a particular obstacle to studying a large number of areas of the hand and long duration sequences. In this work, we propose an automated segmentation methodology that can automatically detect these regions on the hand. This method differs from previous literature because it uses a secondary visual camera and a combination of computer vision and machine learning feature identification. The obtained segmentation models were compared to models segmented by two human operators via Dice and Intersection-over-Union coefficients. The results obtained are very positive: we were able to decompose the images acquired via IRT with our developed algorithms, regardless of the temperature variation, and this with processing times of less than a second. Thus, this technology can be used to study the long-term thermal kinetics of the human hand by automatic feature detection, even in situations where the hand temperature experiences a significant variation.

Keywords: infrared thermography; automated segmentation; real-time; hand segmentation

check for updates

Citation: Arnal, M.; Bourrilhon, C.; Beauchamps, V.; Sauvet, F.; Zahouani, H.; Thieulin, C. An Automated Semantic Segmentation Methodology for Infrared Thermography Analysis of the Human Hand. *J. Sens. Actuator Netw.* **2024**, *13*, 86. https://doi.org/10.3390/jsan13060086

Academic Editor: Lei Shu

Received: 2 October 2024
Revised: 22 November 2024
Accepted: 25 November 2024
Published: 16 December 2024

Copyright: © 2024 by the authors. Licensee MDPI, Basel, Switzerland. This article is an open access article distributed under the terms and conditions of the Creative Commons Attribution (CC BY) license (https://creativecommons.org/licenses/by/4.0/).

1. Introduction

Infrared Thermography (IRT) is a non-invasive method of temperature measurement. It permits the remote study of thermal changes without the need for embedded or attached sensors [1,2]. This method is suitable to the study of the hand's and feet's temperatures [3] and has been used for clinical diagnoses of conditions such as Raynaud's syndrome or rheumatoid arthritis, both of which cause changes in the hand's temperature by altering blood flow. Compared to sensor-based approaches, IRT yields a raw array of temperature values that requires pre-treatment to be effectively utilized, through which the relevant areas of the image are segmented and analyzed. The segmentation step is completed by isolating parts of the thermographic image with shapes known as regions of interest (also referred to as "RoIs"). The layout of these RoI needs to stay consistent throughout; therefore, these regions have to be readjusted between frames. This segmentation is completed manually, imposing a time constraint on the number of thermographic images that can be analyzed. Studies that have utilized IRT for long-term analysis often employ

fixed-sized RoI [4–6], on-skin landmarks [7,8], or lock the area in place [4,9] to address this issue. In the context of environmental testing however, especially when stressors such as intense cold are studied, there is a need for adequate correction of any unwanted motion. This paper aims at helping correct these issues by introducing a new segmentation method to process long IRT sequences (20 min) for the study of the hand's response to cold exposure.

The preliminary segmentation step sets a limit on the ability to process thermographic video sequences. When recording long sequences, parasitic movement may happen and cause subtle changes in pose between subjects. The proper positioning of these regions of interest is necessary in ensuring the reliability of the thermal measurement, as including areas outside of the studied object would skew the results and return incorrect measurements. In the case of neighboring regions in highly heterogeneous areas, positional inconsistency may lower the specificity of each measurement, giving false assessments of temperatures.

Segmentation of a thermal image is comprised of three steps: the extraction of the relevant object from the ambient noise and background information, the decomposition of the object in a series of regions of interest, and the correction of positional errors. The single-channel of thermographic data means that areas with similar temperature values can be extremely hard to differentiate between, as the objects need to have a sufficiently distinct temperature. Non-linear and equalized distributions of colors are another option to accentuate and enhance these fine but consistent difference [10,11]. The difference between the object and the background can be improved by heating or cooling it to provide a sufficient contrast. This can be achieved with a cold surface such as a vat of water [4,12] or a heated surface [13]. The radiation these surfaces emit may interfere with the object or any climate-controlled ambience they may rest in, and excessive difference in background and object temperature may lead to inaccuracy [14]. When studying rewarming or cooling kinetics, the surjective nature of the initial and final temperature evolution across a given period of time can lead to issues in identifying the hand from the background. As the temperature of the studied body reaches values closer to the background's, such as rewarming from near-zero temperature to normothermal ones, areas close to the background will be mistaken with them [15]. IR acquisition may also suffer from inaccurate readings when the image's temperature spans a wide range, especially since the background temperatures would represent a substantial mode in the value distribution of the frame. Additionally, assumptions regarding the temperature of each area may no longer be suitable when studying rewarming or cooling kinetics. Figure 1 highlights these issues with the rewarming kinetic of a hand that has been exposed to cold.

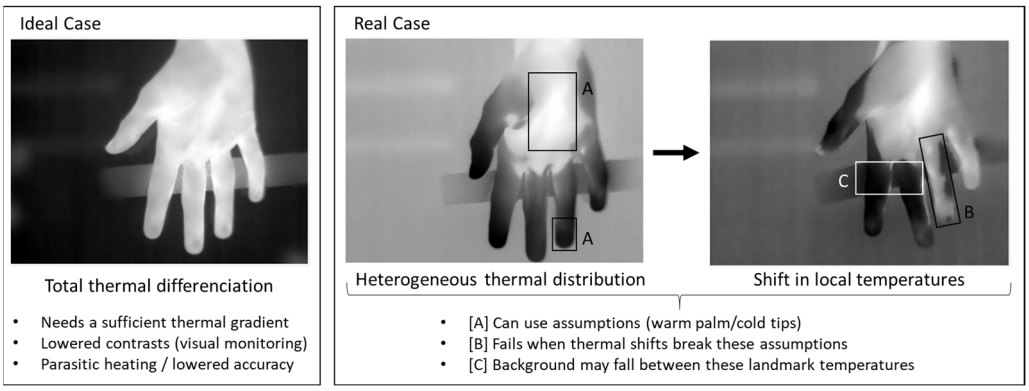


Figure 1. Image illustrating the issues limiting the identification of areas within thermal images, in terms of both object extraction and fine-region segmentation.

Decomposition of the object after extracting it from the background relies on visual cues, which may be amplified by choosing the right palettes and color distribution to increase the contrast along anatomic references. This process is time-consuming, preventing the analysis of large batches of thermographic images, such as videos, long-period changes,

or requiring less exhaustive segmentation patterns. While fixing the object in place is an option for certain applications, this solution may not be adequate for the study of limbs or full bodies due to parasitic motion. Closed enclosures and braces may also disturb the thermal behavior of these systems through conduction. Therefore, automated image segmentation, which can identify these regions continuously without needing to lock the hand in place, would be useful for the study of the hand's thermal behavior.

As such, it is necessary to account for parasitic motion of the hand, and therefore to perform this aforementioned segmentation step either synchronously (for each image of the thermal video feed or of the batch of frames that need to be analyzed) or asynchronously (by checking if the movement or offset between frames is sufficient to need another segmentation of the image). Although repeated segmentation readjustment may be completed manually, this step can also be automated to facilitate the processing of large video files or image batches.

Automated methods of image segmentation have been proposed in the literature, though all rely on thermal data alone to identify these separate regions. These automated methods can be described to identify their shortcomings, as well as the reasons for these limitations.

We can compare and contrast these approaches in regard to (1) how the relevant object data has been extracted from the image, and (2) how the regions were isolated. In the following section pertaining to work related to our research, we present existing studies covering the entire hand and attempting to segment it into marked regions.

Related Work

The first category of works pertaining to the automated segmentation of thermographic images uses classical image processing techniques to identify relevant areas of the hand, using the thermal images themselves as the base for this segmentation. Several examples have been presented in the literature. Common to all these techniques is the use of the thermal data as the source of positional information, either as the raw temperature values or as the false-color render obtained after mapping to a color palette with a set distribution need to have a sufficiently distinct temperature for hand reaching the same temperature.

Kargel et al. [16] utilized a binary masking technique with a temperature-contrasted background to extract the hand. The hand itself was extracted according to cross-correlation with a set reference image. The regions were then isolated by dividing the hand into a warm component (the palm) and a cold component (the fingers) and put in front of a highly emissive background, assumed as isothermal. A dilation operation was used to identify the center of the hand. The fingers themselves could be separated as the complement of this central region of interest according to the position of each fingertip relative to the vertical axis.

This analysis proposal acknowledged the isothermy between sections of the fingers and the background. Using the distribution of temperatures and setting cutoff thresholds on both sides of the peak mode, which corresponds to the quasi-isotherm represented by the background, proved sufficient in separating the palm and fingertips from the background. The fingertips could be further separated by assuming their temperature as lower than the base of the digits, though this may not be sufficient in baseline situations. The use of a set threshold and the assumption that the average value of these regions would remain sufficiently different to ensure their true separation put a limit on the ability to resolve complex thermoregulation behavior. The distribution of temperatures of the hand may not be concentric along the fingers, but instead follow more complex arterial patterns [17]. Heterogeneities induced by blood flow in tissue could normalize these temperatures, leading to uneven RoI sizes. If the offset is reached, the algorithm will not be able to differentiate between the core of the hand and its digits. This method nonetheless presents the use of distinct thermal ranges for the identification of each region, as well as the limitation stemming from their use.

Zhang et al. [18] utilized a modified version of the Otsu algorithm [19], which computes the segmentation thresholds automatically. The modifications involve the use an array of cells to determine specific thresholds for each region. A temperature-controlled

plate was used to provide an isothermal background to help separate the hand. Otsu's method [19] was described for adaptive outlining of the hand in literature [20] and is highly suitable considering the heterogeneous distribution of temperatures within the hand. The extraction of each region was completed with an erosion-dilation morphology operation, which identified the distal and palmar aspects, but limit the segmentation to only these regions of the hand. These steps also depend on an external factor to accurately identify these regions, which is the radius of the fingertips. Comparing the coordinates of each fingertip's center allows for the precise identification of each digit. Patterns that only target the palm and distal regions are common in manual segmentation RoI layouts [4,21]; however, adapting this algorithm to identify regions within the palm or along specific phalanges would require additional positional parameters. It should be noted that this method was tested in a situation where the hands were fully distinct from the background, which may not be the case when studying rewarming or vasodilative patterns. Nevertheless, the modification of Otsu's algorithm with an array of smaller cells would provide more effective separation and solve the issues presented in the first method [16]. This method utilizes the morphological differences between the palm and fingertips to identify these regions from a background-isolated thermal image. Pauk et al. [17] utilized a graph-building algorithm to construct a model of the hand as a series of axes running along the length of the digits, similar to the aforementioned erosion-dilation operation. The use of a whole-image histogram binarization method led to segmentation artifacts due to parts of the hands being colder than the background.

Knish and Rabin [22] included convex-hull detection methods to highlight each finger's most distal point and the angles between them, highlighting the length of each finger and providing further positional data. This methodology allows for the more accurate identification of the phalanges, though still requiring a distinct background temperature. The convex-hull segmentation method used by Knish and Rabin has been utilized for hand-gesture recognition with non-thermal cameras [23], and provides adequate separation of the palmar and digital aspects of the hand in the context of thermal imaging alone [24].

All of these automated methods are vulnerable to the surjective nature of the initial and final temperature evolution across a given period of time. As the temperature of the studied body reaches values closer to the background, such as rewarming or cooling patterns, areas close to the background will be confounded with them.

Having outlined these previous automatic segmentation proposals, we have concluded that the use of thermal data alone is not sufficient for the identification of the hand's features. This is especially true in the context of cold exposure, in which the hand's thermal layout may be highly variable. The use of a visual reference would also provide more flexibility in regard to segmentation layouts. Additionally, traditional segmentation techniques may not effectively distinguish between phalangeal regions, as the use of visual landmarks on the hand would be a way to improve the reliability and consistency of these segmentation patterns.

The second category of automated segmentation works utilize an external visual reference, provided by a secondary sensor mounted parallel to the main thermal camera. This method of segmentation is more robust to temperature changes, though differences remain in regard to the image processing techniques used for the identification of each region of interest.

This dual-sensor method has been described in literature by Smieschek et al. [25], in which a pair of thermal and visual cameras were used to identify distinct features in thermal images. The used layout provides a complete segmentation of the fingers in three phalanges using convex-hull segmentation, though intradigital segmentation is performed by simple division of the fingers themselves. Variability in phalangeal length [26] could lead to false segmentation results. Different poses were also not described in this article, and the experimental setup required separate visual and thermal cameras that could lead to desync issues when analyzing recorded sequences. The difference in phalangeal lengths is more problematic, especially in regard to consistency of measurement and shape of each region of interest.

In order to account for these morphological differences, and to more effectively identify the hand and its features, machine learning-based segmentation may be used, as described in a paper by Wang et al. [27] expanding upon the work completed by Smieschek et al. [20].

Instead of classical computer-vision steps, a deep-learning neural network was employed in this method, trained according to a set segmentation layout.

Therefore using visual references would be more dounded, effective separation and solve the issues presented in is a best*cDeep-learning is effective in its ability to identify specific areas, though at the cost of training time, the ground truth that this study utilized was also segmented manually, and the application of IRT for temperature measurement wasn't the focus of this particular work e focused and clearer waye viewer for these comments and improvement proposals, as they helped us rewrite the manuscript in a m. This latter point is important, as the regions of interest used to segment each area of the hand should be selected to limit curvature or incidence and remain consistent in size and shape throughout the entire sequence [28–31].

Table 1 provides a summary of each of these aforementioned techniques, highlighting the goal that motivated their design, as well as the intrinsic limitations they present. Some of these techniques, for instance, are intended for the diagnosis of certain conditions, therefore focusing on specific aspects such as the arterial patterns of the hand or the general flow patterns across the digits. Another issue stems from the reliance on prior thermal differentiation of the background and hand, or on colorized thermal image renders to identify the hand and its inner regions. The use of non-normalized regions of interest, and the lack of consideration for edge effects, may also lead to incertitude in the measurement of the temperature. Finally, the segmentation patterns presented in these works may not be suitable for the thorough analysis of the hand's thermal behavior, as they only focus on the distal aspects, or do not differentiate between each digit in a reliable manner. Nevertheless, the study of these prior works is useful in determining which analysis method should be employed.

Table 1. Comparison of each related work cited in this introduction, in regard to their hand and feature extraction methods, as well as their limitations.

Article	Positional Data Source	Object Extraction	Region Segmentation	Purpose	Limits
[16]	Thermal Data	Cross-Correlation	Dual Thresholding	Fingertip/Palm temperature	Assumes homogeneity
[17]	Thermal Data	Balanced Histogram Thresholding	Depth-First Search	Diagnosis (Arthritis)	Requires controlled background Diagnosis-Focused
[18]	Thermal Data	Otsu's Thresholding	Erosion/Dilation	Fingertip/Palm temperature	Requires controlled background Assumes homogeneity
[22,24]	Thermal Data	Color Palette Extraction	Convex-Hull	Biometric Identification	Assumes homogeneity. Unsuitable for thermal monitoring
[30]	Thermal Data	Color Palette Extraction	k-Means Clustering	Diagnosis (Arthritis)	Inconsistent Region Size Unsuitable for thermal monitoring
[29]	Thermal Data	Local-Adaptive Thresholding	Hough/Morphological	Diagnosis (Peripheral Vasc)	Requires controlled background
[28]	Thermal Data	Color Palette Extraction	Hough Transform	Temperature Monitoring	Requires controlled background
[25]	Visual Data	Otsu's Thresholding	Convex-Hull	Temperature Monitoring	Prone to edge effects
[20]	Visual Data	Deep-Learning	Deep-Learning	Hygiene monitoring	Unsuitable for thermal monitoring (edge effects)
Our Research	Visual Data	Histogram Extraction	Landmark-based Machine Learning	Temperature Monitoring	Requires colored background/lighting

Our research utilized visual data for the identification of each region, a machine learning framework for the detection of fine landmarks, and classical image segmentation techniques to isolate the hand from a set background. The regions of interest we have acquired are defined as polygonal zones located on each phalange as well as the volar and metacarpal aspects of the hand. The prevalence of these zones is not linked to arterial blood flow or any other specific warm or cold phenomena; as such, they may be resolved even in baseline or low-difference situations. Our methodology is also focused on the study of fine thermal behavior of the phalanges at both the proximal, median, and distal areas, and is designed to focus only on the planar regions of these phalanges by clearing away from the edges of the digits.

The lack of standardization in regard to thermal layouts is a limit to the cross-analysis of studies involving IRT, especially in regard to highly variable regions such as the hands and digits [32]. A common aspect of all these thermal segmentation proposals is their delimitation of the palm of the hand and its digits, motivated by their thermal properties as well as their morphological differences. Therefore, we have aimed for the finer analysis of the hand's digits, from their metacarpal region to their tips, utilizing anatomical reference points. Focusing on the digits, which are slimmer and more prone to parasitic movement, solves the issue of measure repeatability in the context of long video captures. Another aspect common to these studies is a specificity for the distal region of the fingers, with some studies [3,33] measuring only the distal portions of the fingers. In order to provide a more thorough segmentation of the hand, we decided to extend this phalangeal identification to the median and proximal segments of each digit. Doing so would allow for the study of vasoconstrictive effects and an estimate of cutaneous vascular conductance changes within the digit [34,35].

2. Materials and Methods

Our proposed segmentation methodology used the secondary visual sensor of a thermal camera, Aachen, Germany, similar to the setup presented by Smieschek et al. [25] but with more favorable optical parameters. The use of a second visual sensor to provide segmentation data for non-visual range data has been described in the literature [20,27]. Our proposed solution was, however, focused on IRT analysis of the hand, using polygonal RoIs for gradient analysis and clearing away from the non-planar edges of the digits.

A dedicated experimental setup was used for the joint capture of both thermal and visual images. A thermal camera (FLIR A700-EST, FLIR AB Systems) was mounted on an adjustable downward-facing camera mount. The EST variant allows for the dual streaming of both frames. The camera was equipped with a narrow-angle optic (24°, f/.0), giving the infrared imager the same optical characteristics as its visible-range camera. Both thermal and visual frames were acquired with a computed connected to the camera via a Gigabit-Ethernet cable, providing power to the camera via PoE.

The hands were unsupported above the styloid process and were held at a 150 mm distance above a blue background. Thermal emissivity was taken as 0.98 [14]. The hands were kept in a thermally controlled box and illuminated by two white LEDs (2W) located above the observation window. Care was taken to keep the thermal camera at a consistent distance (d = 0.60 m) from the observed hand. The two LEDs were situated beneath a thermally insulating cover and had sufficiently sized heat dissipaters to prevent the camera from being negatively affected by the local heat spot of their die. The illumination angle had a normal incidence to the hand, ensuring that all features were evenly lit, further preventing the disruption of the hand's thermoregulation.

The color of the background was tested utilizing a series of printed sheets and comparing the histogram curves, in order to find the most favorable color. A matte black background was tested (Canson, Black, 160 g/m^2), though concerns about it heating up from the illumination of both LEDs motivated the use of a dark-blue background. The shade of background was chosen as a compromise between attenuation of shadows and sufficient contrast between the hand and background.

A custom camera driver was written with the C# library FLIR Atlas to simultaneously acquire thermal images as well as visual frames. This program had to be written as no solution that could both record and stream visual data was available. Singular image acquisition automatically embeds the visual component in the outputted file's metadata. Sequence acquisition periodically captures the visual image upon reception of a new thermal frame, appending the timestamp of the received infrared frame to an indexing file that keeps track of the index of the visual frame.

While this choice is less efficient that outputting the visual frames to a dedicated video codec, the immediate correspondence between the thermal video's timeline and the index of each frame increases its resilience to signal losses. Uniformity calibration also leads to frame drops in the thermal feed but not its video feed, which could lead to desync issues. Saving each frame individually is less efficient as the file management does not append the image pixel data to a specific stream, instead writing an entire file, including its metadata and header. This additional work leads to an average recovery rate of 70% for the visual feed, dropping to 50% for a USB link. These figures are sufficient for live tracking, as the base framerate of both visual and thermal sensors is a consistent 30 frames per second. Thus, the loss in frames still provides enough visual data to keep track of parasitic motion, drift, and positional readjustment.

The frame loss is also consistent across the video feed, as the GigE Vision protocol employed by this camera for the video streaming is not negatively affected by motion. In the case of fast movements, the effect of thermal feed motion blur may be detrimental to any accurate readings. This timestamping methodology allows for the assessment of the thermal value of the nearest still frame. The distance between the visual and thermal sensors was considered to be narrow enough that stereoscopic compensation would only entail shifting the visual image a few pixels laterally. The visual and thermal sensors were equipped with optics that provided similar angular fields of vision.

Only the visual component was utilized for the segmentation. Stereoscopic effects, caused by the offset between both visual and infrared imagers, were identified using an edge-detection method and coincidence. The visual image was then offset to be aligned with the thermographic image. In the case of mismatched optics, the image was readjusted through homothetic reduction followed by cropping.

Analysis of the images was completed utilizing a C# program for the processing of thermographic images, their synchronization to each visual frame, and the extraction of thermal values from the RoI pattern. This C# program is based on the FLIR ATLAS SDK, which can read IRT sequences (in the proprietary csq format), access embedded metadata in IRT frames (which contains the visual image), and perform the cropping and homothetic readjustment tasks. A Python script was then used to extract the RoIs automatically from each visual image and send them back to the C# IRT analysis program. The IRT analysis program can then obtain the temperature metric for each RoI. The following section describes the tasks performed for the segmentation of the hand.

The tasks performed by the segmentation of the acquired frames, and summarized on Figure 2, rests upon two separate resources, a robust anatomical landmark detection machine learning tool, and the isolation of the hand's contour for surface analysis. The use of deep-learning neural networks for image segmentation in the medical field is an effective method of semantic RoI assignation [36]; however, this combined method is proposed thanks to its flexibility and as a proof of concept. Prior art has highlighted the use of neural networks to segment images as an improvement from classical image processing tasks [37,38], though these utilized static images for which careful tracking was not an issue. Automated segmentation of IRT sequences has been tried with classical examples, with minimal references to this combined approach. One such approach has been described by Wang et al. [35], utilizing this combined convex-hull/landmark detection method to segment the hand. Our approach differs in its use of visual references and its specificity to the hand's phalanges, providing consistent region size regardless of their temperature and a more exhaustive description of the behavior of each digit. Instead of assuming that the

segmented regions will be thermally different at all times, our approach can segment them regardless of temperature and without the need of a specific background temperature. The use of a landmark detection task also provides identification of each phalange according to visual references instead of relying on morphological transforms. Individual detections are shown in Supplementary Datas.

Firstly, images were acquired by putting the object in front of a monochrome background. A dark-blue background was chosen, its darker hue helping limit the contrast between projected shadows and the background color. The first step of the analysis was an edge-detection method (Figure 2II), performed with a Gaussian blur operation then by converting the image to its HSV values, as the high-saturation background can then be extracted from the hand independently of the subjects' phototype. Determination of the hue was completed by capturing the distribution of the frame before insertion, then performing modal analysis to find the most prevalent tints. The maximum and minimum were then used as threshold values to extract the hand from the rest of the frame. Canny's edge detection operator was selected as it provides optimal edge detection and can be easily adapted to situations where the background may not be perfectly even in color or tone.

Secondly, a hand landmark recognition framework was used to provide positional references for the extraction of the hand's phalanges and palm. The tool used for digit detection was a hand-tracking task embedded within the Google Mediapipe framework [39,40]. This task provided a constellation of points that correspond to the joints of the fingers, the metarcarpus, and the thenar eminence of the hand. Mediapipe has been used in other contexts that require careful tracking [41] and has been validated via mediapipe -mapping with homoethetic images [20,42].

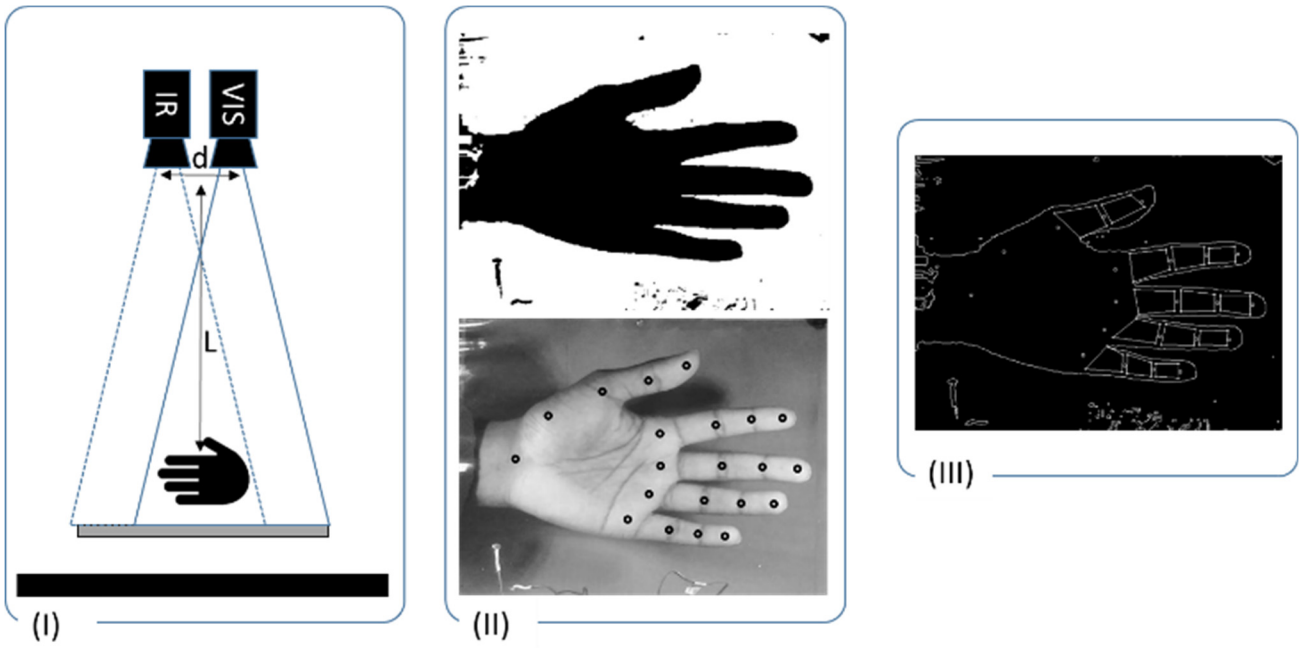


Figure 2. Summarized decomposition of the segmentation process: (**I**) Simultaneous IR/Visible image capture, (**II**) Background removal and feature detection, (**III**) Region segmentation.

These latter examples are important as they combine the punctual constellation obtained via the Hand task with a secondary sensor. Mediapipe is also under the Apache license, facilitating its modification and enhancement. The anatomic segmentation pattern it outputs also presents a high similarity to previously used RoI layouts in infrared thermography of the hand, which focus on the phalanges of the fingers [43–45].

This task, referred in the literature as GMH (Google Mediapipe Hands), detects the junction between each knuckle as well as the tips, carpal, thenar, and hypothenar regions, as discrete points in the image. After retrieving these landmarks, the points were then

expanded to isolate the area of each phalange within the image, using an edge-detection method to extract the hand's contours from the extracted binary mask.

The vertices of each phalange polygon were acquired by detecting the nearest point to the GMH location on the edge (Figure 3a), and then performing a central symmetry operation to detect the opposite edge (Figure 3b). Proximity analysis on this symmetric point was then completed to ensure that each vertex lays on the hand and not outside of it (Figure 3c). A slight homothetic reduction operation was performed, shrinking it to 90% of its size, to clear away from the curved edge of the fingers [46,47] (Figure 3d). A verification step was also completed on the second nearest point detection, in the event that the returned point detects the starting edge as its closest edge. This ensured that the polygon is open and encompasses the phalange.

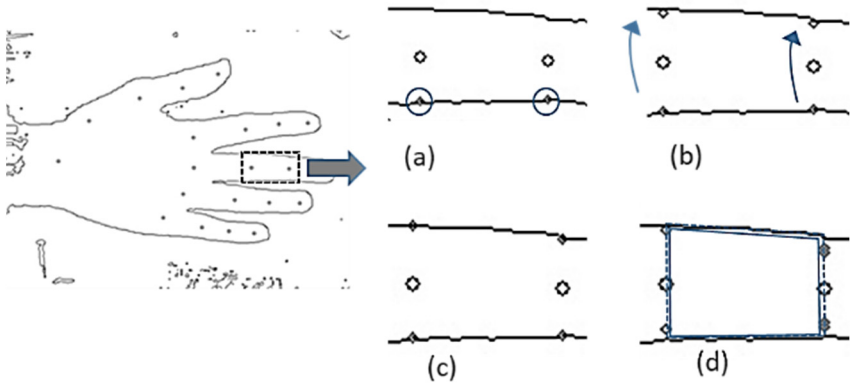


Figure 3. Steps for the construction of phalangeal RoI. (**a**) detection the nearest point to the GMH location on the edge. (**b**) central symmetry to detect the opposite edge, (**c**) proximity analysis and (**d**) slight homothetic reduction.

Proximal areas were detected according to the metacarpal landmarks performing a projection operation along the metacarpal-proximal segment with a slight reductive factor applied to obtain the middle of the base of the digit. The nearest point and its symmetrical point were then calculated, and the middle point of the digit was used to complete the proximal region of interest (Figure 4a).

Due to the curve of the edge of distal phalanges, a projection operation was performed to isolate and identify them (Figure 4b). Utilizing the a fore mentioned method would yield irregularly shaped regions of interest, highly trapezoidal instead of rectangular with a variable base-to-base ratio (Figure 4c). Therefore, the offsets between the median and distal joints along the x and y axes were computed and applied to the points along the contour (Figure 4d).

In the case of fingertip identification, the distal region of interest can be used to calculate the radius of the finger, providing the center and radius of the RoI. This radius may then be used for subsequent frames. Processing time may be further saved by storing the positional data of the MediaPipe-derived constellation and comparing it between frames [42]. Sufficient deviations should then trigger the redefinition of the RoI pattern, improving the time efficiency of the segmentation algorithms. Once the hand is segmented, the extracted coordinates of each RoI can be passed to an IRT program as a formatted file or parsed by an IRT SDK (such as FLIR Atlas SDK in this application).

Testing the performance of the segmentation algorithm was completed by comparing its outputted segmentation patterns to those identified by human operators. This gave us a ground-truth baseline as well as an external reference. Our image dataset was obtained from a local cold-exposure experimental session during which 24 participants were asked to put their hands in a climate-controlled exposure equipped with an observation window and monitored via a thermal camera (as described previously). Each session lasted for a duration of 20 min at most, and each participant did this test four times. This provided a

baseline of 86 different sequences, due to some participants being removed from the study due to medical and scheduling concerns.

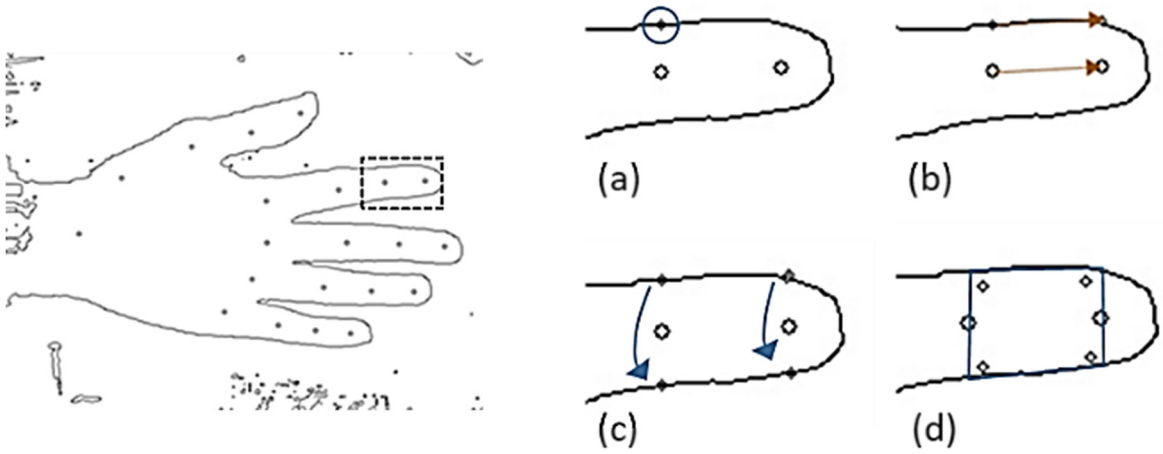


Figure 4. Steps for the construction of distal RoI. The length of the median phalange is used to determine the outline of the fingertip, as the curvature could lead to non-parallel sides as the tip would be narrower than the base Steps are: (**a**) proximal areas detection, (**b**) projection operation, (**c**) trapezoidal symmetry to detect the opposite edge, and (**d**) contour determination.

From this batch, a series of hand images (n = 24) of various morphologies and phototypes were acquired, with each volunteer putting their hand underneath the described setup. Our system is designed for IRT and therefore the images have to comply with experimental requirements to ensure accurate measurements [1,48]. Two operators, one familiar with the segmentation of the hand (referred to as *Trained*, and considered as the ground truth), and one unfamiliar (referred to as *Untrained*), were tasked with the segmentation of the image corpus. They were asked to segment the same starter images with the proposed segmentation pattern, using highly saturated polygons (blue and red at zero, green channel at its fullest), which were then extracted as a binary mask. This gave two datasets of ground truth. Manual segmentation was performed on the visual images, providing optimal conditions for the operators as the recognition of their landmarks was not hindered by thermal ambiguity or loss of detail.

Accuracy and precision tests were performed using the OpenCV image processing library, using the two references (Trained, Untrained) and the automated segmentation layout. The entire RoI constellations were compared first, then the proximal, median, and distal phalanges were analyzed separately. A preliminary bounding step was performed on the hand and digits, isolating the digits for the per-phalange analyses. Doing so reduced the number of pixels that needed to be compared, also increasing the specificity of these tests. A second, smaller bounding box was then applied to the fingers themselves when comparing the phalanges specifically, further reducing the size of the area and increasing the significance of the coefficients. Within these bounding boxes, two comparison tests were performed to check the reliability of the Automated segmentation method: The Sørensen–Dice coefficient, and the Intersection-over-Union (IoU) [49]. The Dice coefficient was used to assess how much the regions obtained by each segmentation pattern matched their position on the hand by measuring the overlap. The IoU provided a stricter assessment by relating this overlap with size discrepancies or offsets between regions. A third metric, referred to as the Pixel Ratio, or number of selected points divided by the number of background pixels, was used to determine how strict each segmentation pattern was in regard to their size.

Statistical analysis of the segmentation coefficients was performed using Jamovi (Version 2.5.5.0) to extract the descriptive statistics of each comparison pair as well as detecting any significant effect and difference between the groups. A Levene test was used to verify the homogeneity of variances and select the appropriate ANOVA, using a

Welch ANOVA for cases with these inhomogeneous distributions and a Fisher ANOVA otherwise. Further identification of these differences was completed with a post hoc test (Games–Howell for inhomogeneous pairings, Tukey for homogeneous pairs).

The one-way ANOVA was used to verify if the differences in segmentation metrics were significant enough at each specific location; this would detect whether or not these differences were also found between trained and untrained operators. Post hoc tests then allowed us to check which group was an outlier or if each were different from each other. The separation between each phalange group was kept, and it was deemed required because of the difference in segmentation tasks between the distal, median, and proximal regions. The significance level of each p-value range was highlighted in the tables ($p < 0.01$: *, $p < 0.005$: **, $p < 0.001$: ***).

3. Results

We used the Sørensen–Dice coefficients [49] to determine the similarity of the automated segmentation output with the two patterns proposed by both operators. These were calculated between these segmentation layouts using a Python script. Table 2 highlights coefficients for all regions.

Table 2. Dice similarity scores for both the entire RoI layout and each range of phalange (Proximal/Median/Distal), higher scores indicate more similar patterns.

Region	Trained-Automated	Untrained-Automated	Trained-Untrained
Full	0.965 ± 0.013	0.971 ± 0.005	0.968 ± 0.014
Proximal	0.843 ± 0.02	0.82 ± 0.022	0.971 ± 0.01
Median	0.972 ± 0.01	0.970 ± 0.005	0.977 ± 0.005
Distal	0.974 ± 0.01	0.966 ± 0.01	0.971 ± 0.007

High Dice similarity coefficients were consistently reported between the two human operators, as well as with the automatic segmentation proposal. A more specific description of these segmentation patterns can be achieved by using a one-way ANOVA between each pair to check which pairing is more statistically different. The full pattern, median, and distal score pairs followed a homogeneous distribution according to Levene's score ($p = 0.128$, p =0.86, $p = 0.686$ respectively) whereas the proximal score pairs had lower p-values indicating a difference in distribution ($p = 0.007$).

The ANOVA scores highlighted a statically significant heterogeneity in the groups for the median regions ($p < 0.01$) but not for the distal scores ($p = 0.066$) or the entire layout ($p = 0.102$). A statistically significant difference was also seen on the proximal pairs ($p = 0.01$). Considering these differences, we further characterized these differences through a post hoc test, whose results are presented in Table 3 for each pair.

Table 3. Mean differences and p-values for each comparison of similarities, highlighting whether or not these differences in segmentation RoIs are significant.

Region	Base-Comparison	Untrained-Automated	Trained-Untrained
Proximal	Trained-Automated	-0.007 ($p = 0.038$) *	-0.01 ($p = 0.05$) **
	Untrained-Automated		-0.003 ($p = 0.359$)
Median	Trained-Automated	0.002 ($p = 0.387$)	-0.005 (p= 0.008) **
	Untrained-Automated		-0.008 (p< 0.001) ***

* Is $p < 0.05$, ** $p < 0.01$ and *** $p < 0.001$.

Post hoc pairwise comparisons highlighted differences in the way each region was segmented. The highest statistically significant differences were found in the median phalanges, followed by the proximal phalanges. Further characterization can be achieved

by analyzing the size of each region relative to the bounding box, as larger selected regions may indicate a less-strict segmentation.

Considering this, pixel counts within these regions were compared by calculating the ratio between the number of pixels comprising the RoI, and those comprising the background. Higher ratios indicate that the segmentation outputted larger regions. Table 4 presents these values according to the specific areas of the RoI.

Table 4. Pixel ratios (selected pixels/pixels of the bounding box) for each segmentation proposal and region. Higher scores indicate that the segmented patterns encompassed larger zones, whereas lower scores indicate a stricter segmentation.

Region	Trained	Untrained	Automated
Distal	0.074 ± 0.012	0.09 ± 0.01	0.065 ± 0.01
Median	0.097 ± 0.0145	0.1 ± 0.014	0.092 ± 0.012
Proximal	0.12 ± 0.02	0.11 ± 0.019	0.097 ± 0.015
Full	0.16 ± 0.03	0.16 ± 0.03	0.13 ± 0.02

The automated layout presents a slightly lower ratio in the proximal and distal regions, highlighting a tendency to output smaller RoIs, or a more conservative estimate of the size of features.

Identifying the cause of these variations in background rejection ratios can be completed by assessing the Intersection-Over-Union Index, which is specific to the segmented pixels of the automated layout. The Intersection-Over-Union Index provides more insight on the slight variations and heterogeneities, emphasizing the overlapping and extra pixels a particular segmentation layout may have. Table 5 presents the IoU scores for each region, as well as the spread of these values.

Table 5. Intersection-Over-Union Index for every segmentation comparison and region. Higher scores indicate that the patterns had minimal mismatch.

Region	Trained-Automated	Untrained-Automated	Trained-Untrained
Full	0.61 ± 0.055	0.66 ± 0.03	0.67 ± 0.06
Proximal	0.65 ± 0.07	0.69 ± 0.03	0.74 ± 0.05
Median	0.73 ± 0.05	0.71 ± 0.04	0.78 ± 0.05
Distal	0.69 ± 0.05	0.64 ± 0.05	0.69 ± 0.05

The IoU score stayed consistently above the 0.5 limit but highlighted some irregularities and issues. The same aforementioned one-way ANOVA and post hoc test process was performed, highlighting differences across all regions and highly heterogeneous scores for the distal phalanges. Table 6 presents these differences between pairings.

Table 6. Mean differences and p-values for each comparison of IoU scores, showing the lines for which the one-way ANOVA returned a significant result.

Region	Base-Comparison	Untrained-Automated	Trained-Untrained
Proximal	Trained-Automated	-0.0419 ($p = 0.023$) *	-0.09 ($p < 0.001$) ***
	Untrained-Automated		-0.048 ($p = 0.008$) **
Median	Trained-Automated	0.012 ($p = 0.653$)	-0.0587 ($p < 0.001$) ***
	Untrained-Automated		-0.0706 ($p < 0.001$) ***
Distal	Trained-Automated	0.047 ($p = 0.004$) **	
	Untrained-Automated		-0.0466 ($p = 0.004$) **

* Is $p < 0.05$, ** $p < 0.01$ and *** $p < 0.001$.

The Intersection-Over-Union scores were the highest for the trained-untrained segmentation pattern pairs, indicating high similarities between these patterns. Lower similarity scores were found with the automated segmentation pattern, though still above the 0.5 limit. High statistical significance was found in the differences between all patterns in the proximal phalanges, and in the median phalanges with the automated layout.

4. Discussions

The presented methodology does not use the thermal data of the IRT frames for their segmentation, unlike prior works. This provides immunity to temperature changes within the hand, which could prevent the separation of the hand from the background. The use of a color-coded background rather than thermal thresholds allows this separation regardless of temperature changes. Using visual references instead of thermal references also allows for the segmentation of the digits into their phalanges at every temperature level. Prior works that have attempted to automatically segment the digits either focused only on the fingertips or had undefined zones at the base of the digits, with fixed RoI radii [18] or the assumption that the fingertips would always be colder than the base of the hand [16]. Works that have used visual sensors for segmentation used only a binary mask to separate the hand and then relied on morphological transforms to isolate each region [25]. Our present method instead uses on-hand landmarks to extract each region, regardless of pose. The movement of each landmark may also be used to quantify the amount of motion between frames and therefore whenever RoI readjustment is needed.

Compared to methods that utilize classical segmentation approaches [16,18], our method is immune to thermal changes of the hand, utilizes actual landmarks to separate each region without anatomical or thermal assumptions to identify them, and can limit the influence of edge effects that can negatively affect the accuracy of measurement.

The review of the segmentation performance metrics was favorable, with the Dice similarity coefficient pointing toward a high equivalence between both operators and the automated segmentation program. The scores were slightly lower between the automated segmentation patterns and both trained/untrained operators at the proximal and median phalanges. This difference is also noticeable in the Intersection-Over-Union tests, though the similarity scores between the trained operator and automated segmentation patterns were higher than between the untrained operator and automated segmentation. This difference is especially present in the proximal and distal regions.

The segmented pixel to background ratio was higher for the trained/untrained operators than the segmentation layout outputted by our tool. This effect may be caused by the homothetic reduction step as well as the propensity to over-estimate phalange length by utilizing the folds of the phalangeal joints as the distance reference. Similar effects were not found to be significant in the median regions. Slightly smaller regions of interest may not be problematic in the context of spatial averaging of thermal values, provided they are still large enough to account for optical effects and sensor non-uniformity [50]. When checking the IoU index, dissimilarities between segmentation patterns were more pronounced at the proximal areas, which are caused by the difficulty to adequately identify the metacarpal limit and base of the fingers. This problem way be solved by using the aforementioned morphological reduction-then-dilation operation [18] to isolate the palm and therefore accurately define that palmar-proximal limit. In this context, the combination of classical computer-vision techniques with machine learning feature identification provides an effective segmentation solution.

This methodology utilizes less hardware but is limited by the need for a visually distinct background. Extraction of these subdivided regions of interest was one of the goals of this segmentation layout, but semantic segmentation methods based on deep-learning are more agile in terms of possible layouts. Processing times may also be assessed when compared to DL-based segmentation, as the number of pre-treatment operations could lead to a considerable overhead. Considering this, we aim to switch to a full deep-learning approach by using the data acquired from this run and the segmentation patterns we have

obtained from this methodology. Increasing the training set will be completed by altering the base images through rotation [37,38] and by using the monochrome background as a chromakey to provide alternate background conditions [51].

Limitations are the small size of different samples (n = 24) and the use of a dedicated colored background. Infrared Thermography does require a uniform background to ensure the accuracy of measurements [14], making this issue less problematic. Sufficient lighting is necessary to prevent shading effects from affecting the background separation, as described by Smieschek et al. [25]. We used LED lighting, providing minimal parasitic infrared radiation that would otherwise decrease the accuracy of the read temperatures. The frames came from recorded sequences, each lasting 20 min and presenting unwanted hand motion. The aim of this project is to correct positional errors emanating from this movement, which ca not be predicted and would therefore need to be readjusted manually. In the context of research IRT, the hand's pose should be consistent and planar, and the observation conditions should be monitored and controlled to ensure accuracy. We are intending, however, to improve this method further by switching to a full DL approach, using our segmentation tool to provide an extensive training dataset.

5. Conclusions

Because the hands are important exchanges surfaces for the thermal regulation of the human body [52], their thermal behavior is therefore of high interest, with thermographic image analysis providing a surface assessment of their temperature distribution. Motion compensation and fast segmentations are two issues hindering the analysis of long-term exposure sequences, exhaustive thermographic kinetics, or complex areas. The hand has a complex structure, containing areas of varying aspect ratios, and a curvature along its digits. Therefore, automatic segmentation solutions developed for its analysis have to account for a variety of morphologies and shapes.

After considering the limits inherent to Infrared Thermography analysis, we have developed a new method to accurately and effectively segment thermographic images and sequences. This method solves the issues presented in prior works, such as the need for a completely distinct thermal background to effectively identify each digit, or the limitation to either the distal or palmar aspects. The method is also capable of adequately identifying the boundary between each phalange and uses more consistent anatomical markers to extract each region. Further improvements to this method include the removal of the need for a color-coded background and the automated coincidence of both visual and thermal images for applications where the optical distance may not be fixed.

Supplementary Materials: The following supporting information can be downloaded at: https://www.mdpi.com/article/10.3390/jsan13060086/s1.

Author Contributions: Methodology, M.A., V.B. and C.B.; software, M.A.; validation, M.A. and F.S.; writing—original draft, M.A.; writing—review and editing, C.T.; supervision, C.B., F.S., V.B., H.Z. and C.T. All authors have read and agreed to the published version of the manuscript.

Funding: This research project was done in the context of a PhD Thesis cofinanced by the Ecole Centrale d'Electronique as well as RACER 1927 company. This research was funded by the General Directorate for Armament (DGA), Ministry of the Armies, grants numbers PDH-1-SAN-1-2311 and PDH-1-MRH-1-2203).

Data Availability Statement: The original contributions presented in the study are included in the article, further inquiries can be directed to Cyprien Bourrilhon (C.B.).

Acknowledgments: We thank Benoit Lepetit and Caroline Dussault for their technical help.

Conflicts of Interest: The authors declare no conflicts of interest.

References

1. Lahiri, B.B.; Bagavathiappan, S.; Jayakumar, T.; Philip, J. Medical Applications of Infrared Thermography: A Review. *Infrared Phys. Technol.* **2012**, *55*, 221–235. [CrossRef]
2. Sousa, E.; Vardasca, R.; Teixeira, S.; Seixas, A.; Mendes, J.; Costa-Ferreira, A. A Review on the Application of Medical Infrared Thermal Imaging in Hands. *Infrared Phys. Technol.* **2017**, *85*, 315–323. [CrossRef]
3. Formosa, C.; Gatt, A. Thermographic Patterns of the Upper and Lower Limbs: Baseline Data. *Int. J. Vasc. Med.* **2015**, *2015*, 831369.
4. Brändström, H.; Grip, H.; Hallberg, P.; Grönlund, C.; Angquist, K.-A.; Giesbrecht, G. Hand Cold Recovery Responses Before and After 15 Months of Military Training in a Cold Climate. *Aviat. Space Environ. Med.* **2008**, *79*, 904–908. [CrossRef]
5. Aguilar-Ferrándiz, M.E.; Casas-Barragán, A.; Tapia-Haro, R.M.; Rus, A.; Molina, F.; Correa-Rodríguez, M. Evaluation of Sympathetic Adrenergic Branch of Cutaneous Neural Control throughout Thermography and Its Relationship to Nitric Oxide Levels in Patients with Fibromyalgia. *J. Therm. Biol.* **2021**, *95*, 102813. [CrossRef] [PubMed]
6. Jones, D.; Covins, S.F.; Miller, G.E.; Morrison, K.I.; Clark, A.G.; Calcott, S.D.; Anderson, A.M.; Lucas, S.J.E.; Imray, C.H.E. Infrared Thermographic Analysis of Surface Temperature of the Hands During Exposure to Normobaric Hypoxia. *High Alt. Med. Biol.* **2018**, *19*, 388–393. [CrossRef] [PubMed]
7. Livingstone, S.D.; Nolan, R.W.; Frim, J.; Reed, L.D.; Limmer, R.E. A Thermographic Study of the Effect of Body Composition and Ambient Temperature on the Accuracy of Mean Skin Temperature Calculations. *Eur. J. Appl. Physiol.* **1987**, *56*, 120–125. [CrossRef] [PubMed]
8. Galvin, E.M.; Niehof, S.; Medina, H.J.; Zijlstra, F.J.; van Bommel, J.; Klein, J.; Verbrugge, S.J.C. Thermographic Temperature Measurement Compared with Pinprick and Cold Sensation in Predicting the Effectiveness of Regional Blocks. *Anesth. Analg.* **2006**, *102*, 598. [CrossRef]
9. Sagaidachnyi, A.; Skripal, A.; Fomin, A.; Usanov, D. Determination of the Amplitude and Phase Relationships between Oscillations in Skin Temperature and Photoplethysmography-Measured Blood Flow in Fingertips. *Physiol. Meas.* **2014**, *35*, 153–166. [CrossRef]
10. Mello Román, J.C.; Vázquez Noguera, J.L.; Legal-Ayala, H.; Pinto-Roa, D.P.; Gomez-Guerrero, S.; García Torres, M. Entropy and Contrast Enhancement of Infrared Thermal Images Using the Multiscale Top-Hat Transform. *Entropy* **2019**, *21*, 244. [CrossRef]
11. Abdul Wahab, A.; Salim, M.; Yunus, J.; Ramlee, M.H. Comparative Evaluation of Medical Thermal Image Enhancement Techniques for Breast Cancer Detection. *J. Eng. Technol. Sci.* **2018**, *50*, 40–52. [CrossRef]
12. Leijon-Sundqvist, K.; Tegner, Y.; Olsson, F.; Karp, K.; Lehto, N. Relation between Dorsal and Palmar Hand Skin Temperatures during a Cold Stress Test. *J. Therm. Biol.* **2017**, *66*, 87–92. [CrossRef] [PubMed]
13. Høiland, I.; Weerd, L.; Mercer, J. The Effect of Oral Uptake of Nicotine in Snus on Peripheral Skin Blood Circulation Evaluated by Thermography. *Temperature* **2014**, *1*, 220–226. [CrossRef]
14. Tattersall, G.J. Infrared Thermography: A Non-Invasive Window into Thermal Physiology. *Comp. Biochem. Physiol. Part A Mol. Integr. Physiol.* **2016**, *202*, 78–98. [CrossRef]
15. Lindberg, L.; Kristensen, B.; Eldrup, E.; Thomsen, J.F.; Jensen, L.T. Infrared Thermography as a Method of Verification in Raynaud's Phenomenon. *Diagnostics* **2021**, *11*, 981. [CrossRef]
16. Blank, M.; Kargel, C. Infrared Imaging to Measure Temperature Changes of the Extremities Caused by Cigarette Smoke and Nicotine Gums. In Proceedings of the 2006 IEEE Instrumentation and Measurement Technology Conference Proceedings, Sorrento, Italy, 24–27 April 2006; pp. 794–799.
17. Pauk, J.; Ihnatouski, M.; Wasilewska, A. Detection of Inflammation from Finger Temperature Profile in Rheumatoid Arthritis. *Med. Biol. Eng. Comput.* **2019**, *57*, 2629–2639. [CrossRef]
18. Zhang, H.-D.; He, Y.; Wang, X.; Shao, H.-W.; Mu, L.-Z.; Zhang, J. Dynamic Infrared Imaging for Analysis of Fingertip Temperature after Cold Water Stimulation and Neurothermal Modeling Study. *Comput. Biol. Med.* **2010**, *40*, 650–656. [CrossRef]
19. Otsu, N. A Threshold Selection Method from Gray-Level Histograms. *IEEE Trans. Syst. Man Cybern.* **1979**, *9*, 62–66. [CrossRef]
20. Wang, C.; Jiang, W.; Yang, K.; Sarsenbayeva, Z.; Tag, B.; Dingler, T.; Goncalves, J.; Kostakos, V. Use of Thermal Imaging to Measure the Quality of Hand Hygiene. *J. Hosp. Infect.* **2023**, *139*, 113–120. [CrossRef]
21. Casas-Barragán, A.; Muñoz-Revilla, A.; Tapia-Haro, R.M.; Molina, F.; Correa-Rodríguez, M.; Aguilar-Ferrándiz, M.E. Vasodilatory Peripheral Response and Pain Levels Following Radiofrequency Stressor Application in Women with Fibromyalgia. *Biomedicines* **2024**, *12*, 142. [CrossRef]
22. Knish, A.; Rabin, N. Thermal Heat Distribution Features for Hand Identification. *Expert Syst. Appl.* **2022**, *203*, 117462. [CrossRef]
23. Yeo, H.-S.; Lee, B.-G.; Lim, H. Hand Tracking and Gesture Recognition System for Human-Computer Interaction Using Low-Cost Hardware. *Multimed. Tools Appl.* **2013**, *74*, 2687–2715. [CrossRef]
24. Faltaous, S.; Liebers, J.; Abdelrahman, Y.; Alt, F.; Schneegaß, S. VPID: Towards Vein Pattern Identification Using Thermal Imaging. *i-com* **2019**, *18*, 259–270. [CrossRef]
25. Smieschek, M.; Kobsik, G.; Stollenwerk, A.; Kowalewski, S.; Orlikowsky, T.; Schoberer, M. Aided Hand Detection in Thermal Imaging Using RGB Stereo Vision. In Proceedings of the 2019 41st Annual International Conference of the IEEE Engineering in Medicine and Biology Society (EMBC), Berlin, Germany, 23–27 July 2019; Volume 2019, pp. 6314–6317.
26. Alexander, B.; Kotiuk, V. Proportions of Hand Segments. *Int. J. Morphol.* **2010**, *28*, 755–758.

27. Wang, C.; Jiang, W.; Yang, K.; Sarsenbayeva, Z.; Tag, B.; Dingler, T.; Goncalves, J.; Kostakos, V. A System for Computational Assessment of Hand Hygiene Techniques. *J. Med. Syst.* **2022**, *46*, 36. [CrossRef]
28. Gauci, J.; Falzon, O.; Camilleri, K.P.; Formosa, C.; Gatt, A.; Ellul, C.; Mizzi, S.; Mizzi, A.; Cassar, K.; Chockalingam, N. Automated Segmentation and Temperature Extraction from Thermal Images of Human Hands, Shins and Feet. In Proceedings of the XIV Mediterranean Conference on Medical and Biological Engineering and Computing 2016, Paphos, Cyprus, 31 March–2 April 2016; Kyriacou, E., Christofides, S., Pattichis, C.S., Eds.; Springer International Publishing: Cham, Switzerland, 2016; pp. 275–280.
29. Gauci, J.; Falzon, O.; Formosa, C.; Gatt, A.; Ellul, C.; Mizzi, S.; Mizzi, A.; Sturgeon Delia, C.; Cassar, K.; Chockalingam, N.; et al. Automated Region Extraction from Thermal Images for Peripheral Vascular Disease Monitoring. *J. Healthc. Eng.* **2018**, *2018*, 5092064. [CrossRef] [PubMed]
30. Snekhalatha, U.; Anburajan, M.; Sowmiya, V.; Venkatraman, B.; Menaka, M. Automated Hand Thermal Image Segmentation and Feature Extraction in the Evaluation of Rheumatoid Arthritis. *Proc. Inst. Mech. Eng. Part H J. Eng. Med.* **2015**, *229*, 319–331. [CrossRef]
31. Danko, M.; Hudak, R.; Foffová, P.; Zivcak, J. An Importance of Camera—Subject Distance and Angle in Musculoskeletal Application of Medical Thermography. *Acta Electrotech. Inform.* **2010**, *10*, 57–60.
32. Ammer, K. The Glamorgan Protocol for Recording and Evaluation of Thermal Images of the Human Body. *Thermol. Int.* **2008**, *18*, 125–129.
33. Park, D.; Kim, B.; Lee, S.-E.; Kim, D.; Eom, Y.; Cho, J.; Yang, J.; Kim, M.; Kwon, H.-D.; Lee, J. Application of Digital Infrared Thermography for Carpal Tunnel Syndrome Evaluation. *Sci. Rep.* **2021**, *11*, 21963. [CrossRef]
34. Rubinstein, E.H.; Sessler, D.I. Skin-Surface Temperature Gradients Correlate with Fingertip Blood Flow in Humans. *Anesthesiology* **1990**, *73*, 541–545. [CrossRef]
35. Sessler, D.I. Skin-Temperature Gradients Are a Validated Measure of Fingertip Perfusion. *Eur. J. Appl. Physiol.* **2003**, *89*, 401–402; author reply 403–404. [CrossRef] [PubMed]
36. Ronneberger, O.; Fischer, P.; Brox, T. U-Net: Convolutional Networks for Biomedical Image Segmentation. In Proceedings of the Medical Image Computing and Computer-Assisted Intervention—MICCAI 2015, Munich, Germany, 5–9 October 2015.
37. Abidin, Z.U.; Naqvi, R.A.; Haider, A.; Kim, H.S.; Jeong, D.; Lee, S.W. Recent Deep Learning-Based Brain Tumor Segmentation Models Using Multi-Modality Magnetic Resonance Imaging: A Prospective Survey. *Front. Bioeng. Biotechnol.* **2024**, *12*, 1392807. [CrossRef] [PubMed]
38. Imran, S.M.A.; Saleem, M.W.; Hameed, M.T.; Hussain, A.; Naqvi, R.A.; Lee, S.W. Feature Preserving Mesh Network for Semantic Segmentation of Retinal Vasculature to Support Ophthalmic Disease Analysis. *Front. Med.* **2022**, *9*, 1040562. [CrossRef]
39. Zhang, F.; Bazarevsky, V.; Vakunov, A.; Tkachenka, A.; Sung, G.; Chang, C.-L.; Grundmann, M. MediaPipe Hands: On-Device Real-Time Hand Tracking. *arXiv* **2020**, arXiv:2006.10214.
40. Lugaresi, C.; Tang, J.; Nash, H.; McClanahan, C.; Uboweja, E.; Hays, M.; Zhang, F.; Chang, C.-L.; Yong, M.; Lee, J.; et al. MediaPipe: A Framework for Building Perception Pipelines. *arXiv* **2019**, arXiv:1906.08172.
41. Ehara, Y.; Inui, A.; Mifune, Y.; Nishimoto, H.; Yamaura, K.; Kato, T.; Furukawa, T.; Tanaka, S.; Kusunose, M.; Takigami, S.; et al. Estimating the Thumb Rotation Angle by Using a Tablet Device With a Posture Estimation Artificial Intelligence Model. *Cureus* **2024**, *16*, e59657. [CrossRef] [PubMed]
42. Amprimo, G.; Masi, G.; Pettiti, G.; Olmo, G.; Priano, L.; Ferraris, C. Hand Tracking for Clinical Applications: Validation of the Google MediaPipe Hand (GMH) and the Depth-Enhanced GMH-D Frameworks. *Biomed. Signal Process. Control* **2024**, *96*, 106508. [CrossRef]
43. Takeda, F.; Moro, A.; Martins, N. Thermographic Images to Measure Health Risks of Workers Exposed to Artificially Refrigerated Environments. *Braz. J. Poult. Sci.* **2018**, *20*, 245–254. [CrossRef]
44. Kingma, C.F.; Hofman, I.I.; Daanen, H.A.M. Relation between Finger Cold-Induced Vasodilation and Rewarming Speed after Cold Exposure. *Eur. J. Appl. Physiol.* **2019**, *119*, 171–180. [CrossRef] [PubMed]
45. Horikoshi, M.; Inokuma, S.; Kijima, Y.; Kobuna, M.; Miura, Y.; Okada, R.; Kobayashi, S. Thermal Disparity between Fingers after Cold-Water Immersion of Hands: A Useful Indicator of Disturbed Peripheral Circulation in Raynaud Phenomenon Patients. *Intern. Med.* **2016**, *55*, 461–466. [CrossRef]
46. Cheng, T.-Y.; Deng, D.; Herman, C. Curvature effect quantification for in-vivo IR thermography. In *ASME International Mechanical Engineering Congress and Exposition*; American Society of Mechanical Engineers: New York, NY, USA, 2012; pp. 127–133. [CrossRef]
47. Fernández-Cuevas, I.; Bouzas Marins, J.C.; Arnáiz Lastras, J.; Gómez Carmona, P.M.; Piñonosa Cano, S.; García-Concepción, M.Á.; Sillero-Quintana, M. Classification of Factors Influencing the Use of Infrared Thermography in Humans: A Review. *Infrared Phys. Technol.* **2015**, *71*, 28–55. [CrossRef]
48. Shin, H.; Khoshelham, K.; Lee, K.; Jung, S.; Kim, D.; Lee, W. Effect of Incidence Angle on Temperature Measurement of Solar Panel with Unmanned Aerial Vehicle-Based Thermal Infrared Camera. *Remote Sens.* **2024**, *16*, 1607. [CrossRef]
49. Müller, D.; Soto-Rey, I.; Kramer, F. Towards a Guideline for Evaluation Metrics in Medical Image Segmentation. *BMC Res. Notes* **2022**, *15*, 210. [CrossRef]
50. Pušnik, I.; Geršak, G. Evaluation of the Size-of-Source Effect in Thermal Imaging Cameras. *Sensors* **2021**, *21*, 607. [CrossRef] [PubMed]

51. Pöllabauer, T.; Knauthe, V.; Boller, A.; Kuijper, A.; Fellner, D. Fast Training Data Acquisition for Object Detection and Segmentation Using Black Screen Luminance Keying. *J. WSCG* **2024**, *32*. [CrossRef]
52. Taylor, E.; Tipton, M.; Caldwell Odgers, J.; Heuvel, A.; Machado-Moreira, C.; Taylor, N. The Roles of Hands and Feet in Temperature Regulation in Hot and Cold Environments. In *Faculty of Health & Behavioural Sciences-Papers*; The University of Queensland: Brisbane, QLD, Australia, 2009.

Disclaimer/Publisher's Note: The statements, opinions and data contained in all publications are solely those of the individual author(s) and contributor(s) and not of MDPI and/or the editor(s). MDPI and/or the editor(s) disclaim responsibility for any injury to people or property resulting from any ideas, methods, instructions or products referred to in the content.